AD A134 758 OBSERVATION OF MAGNETIC FIELDS IN LASER-PRODUCED PLASMA - 1/1
USING THE ZEEMAN EFFECT(U) NAVAL RESEARCH LAB
WASHINGTON DC E A MCLEAN ET AL. 30 SEP 83 NRL-MR-5161

UNCLASSIFIED F/G 20/6 NL

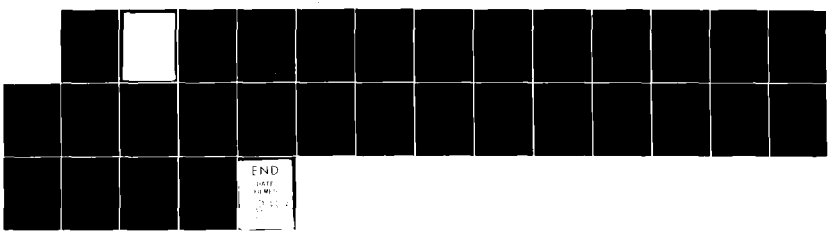

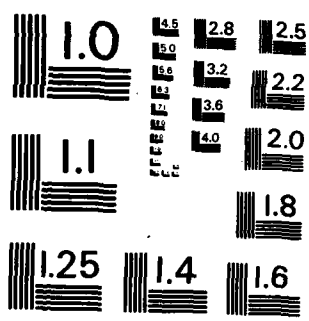

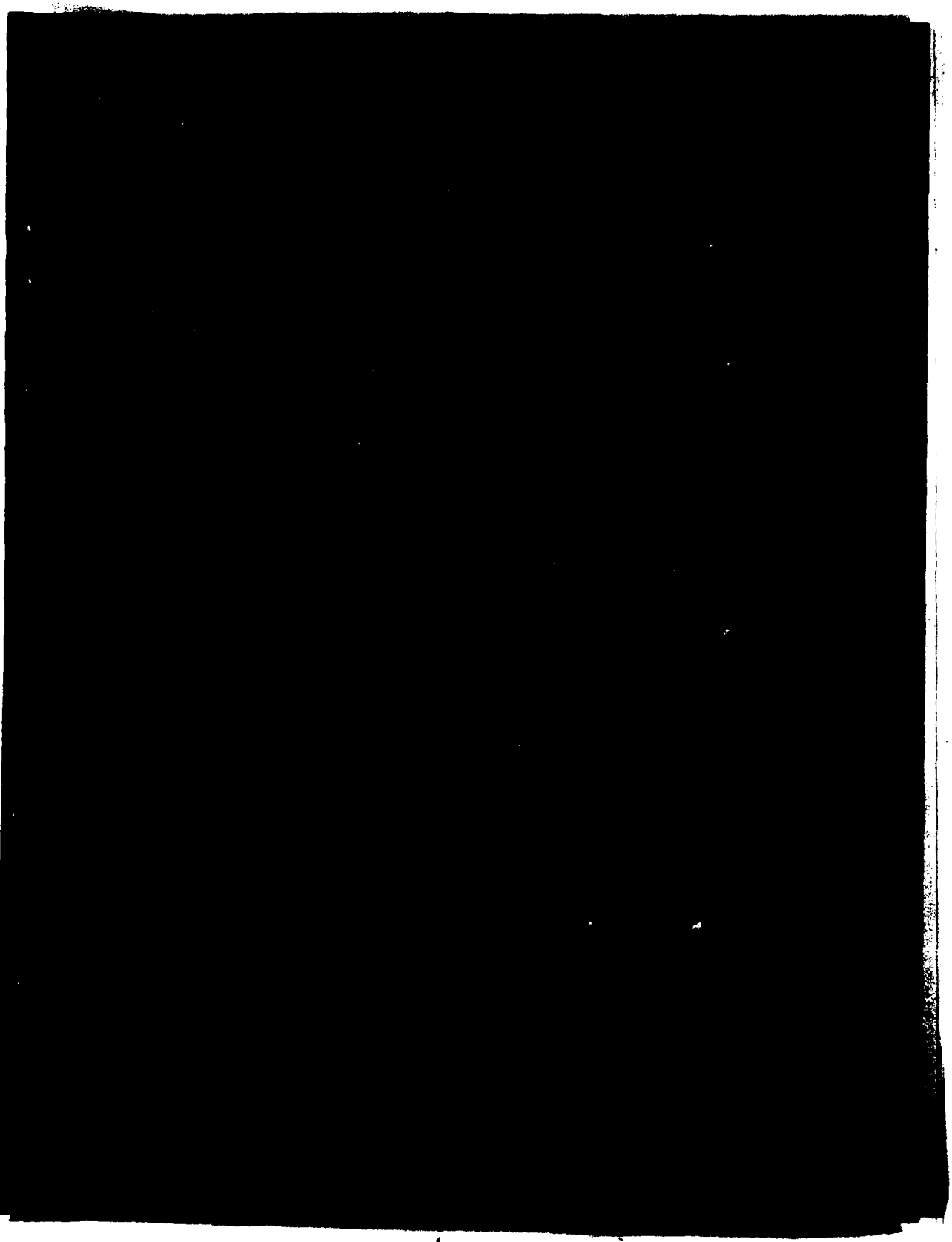

SECURITY CLASSIFICATION OF THIS PAGE (When Data Entered)

REPORT DOCUMENTATION PAGE		READ INSTRUCTIONS BEFORE COMPLETING FORM
1. REPORT NUMBER NRL Memorandum Report 5161	2. GOVT ACCESSION NO. AD-A134758	3. RECIPIENT'S CATALOG NUMBER
4. TITLE (and Subtitle) OBSERVATION OF MAGNETIC FIELDS IN LASER-PRODUCED PLASMA USING THE ZEEMAN EFFECT		5. TYPE OF REPORT & PERIOD COVERED Interim report on a continuing NRL problem. 6. PERFORMING ORG. REPORT NUMBER
7. AUTHOR(s) E. A. McLean, J. A. Stamper, C. K. Manka,* H. R. Griem,** D. W. Droemer,* and B. H. Ripin		8. CONTRACT OR GRANT NUMBER(s)
9. PERFORMING ORGANIZATION NAME AND ADDRESS Naval Research Laboratory Washington, DC 20375		10. PROGRAM ELEMENT, PROJECT, TASK AREA & WORK UNIT NUMBERS DOE AI08-79DP 40092(172); 47-0859-0-3; 47-1606-0-3
11. CONTROLLING OFFICE NAME AND ADDRESS U.S. Department of Energy Washington, DC 20545		12. REPORT DATE September 30, 1983 13. NUMBER OF PAGES 29
14. MONITORING AGENCY NAME & ADDRESS(if different from Controlling Office)		15. SECURITY CLASS. (of this report) UNCLASSIFIED 15a. DECLASSIFICATION/DOWNGRADING SCHEDULE

16. DISTRIBUTION STATEMENT (of this Report)

Approved for public release; distribution unlimited.

17. DISTRIBUTION STATEMENT (of the abstract entered in Block 20, if different from Report)

18. SUPPLEMENTARY NOTES

*Present address: Sam Houston State University, Huntsville, TX 77341.
**Present address:: University of Maryland, College Park, MD 20742.
This work was supported by the U.S. Department of Energy and the Defense Nuclear Agency under Subtask I25BMXI0, work unit 00015, and work unit title "Early Time Plasma."

19. KEY WORDS (Continue on reverse side if necessary and identify by block number)

Self-generated magnetic fields
Zeeman effect
Laser-produced plasmas
Transport phenomena

20. ABSTRACT (Continue on reverse side if necessary and identify by block number)

The self-generated magnetic field produced when a pulsed Nd:glass laser is focused onto a carbon foil target is measured for the first time using the Zeeman effect. Emission from the CV $1s2s\,^3S_1$ - $1s2p\,^3P_2$ (2270.9Å) was used for the measurement. At a laser irradiance of $\sim 5 \times 10^{12}$ W/cm^2, the magnetic field increased from 100 kG to 200 kG when the focal spot was changed from a flat-topped distribution to a ring pattern, which caused higher density gradients. A Faraday rotation measurement at ~ 200 kG agreed with the Zeeman effect measurement. Opacity effects in the plasma enhanced the sensitivity of the Zeeman measurement.

DD FORM 1 JAN 73 1473 EDITION OF 1 NOV 65 IS OBSOLETE
S/N 0102-014-6601

SECURITY CLASSIFICATION OF THIS PAGE (When Data Entered)

CONTENTS

OBSERVATION OF MAGNETIC FIELDS IN LASER-PRODUCED PLASMA USING THE ZEEMAN EFFECT

I. INTRODUCTION

It has been known for some time that a large magnetic field[1] is generated when energetic laser pulses irradiate solid targets. These fields can result from thermoelectric and pressure effects that are present in these laser-generated plasmas, and are a strong function of temperature and pressure gradients within the plasma. Knowledge of these fields is important in studies of laser fusion and interstreaming plasma instabilities due to their effect on thermal transport,[2] absorption, and other processes that occur in these plasmas. For example, recently Forslund and Brackbill[3] have predicted that these large magnetic fields will grossly alter the transport of hot electrons, energy and ions in CO_2 laser-target interactions. A variety of techniques to measure the magnetic fields have already been used, such as small probe coils,[4] Faraday rotation,[5,6] and the imprint on magnetic tape.[7]. However, this paper describes the first application of the Zeeman effect to measure these self-generated magnetic fields in laser-plasmas, and the first observations in the range of 100-300 kG. Those fields are produced by laser irradiances in the range of 10^{12}-10^{14} W/cm^2 and are important in laser ablation studies.

Although magnetic probe coils were first used to measure magnetic fields in laser-irradiated solid targets, they can only be deployed at distances down to a few mm from the target surface (due to the fact that the plasma severly damages the probe) and consequently could only measure fields of a few kilogauss. Also, the magnetic probes perturb the plasma. On the other hand, optical measurements such as Faraday rotation and Zeeman effect do not perturb the plasma and have the ability to measure the magnetic fields at much higher densities. Stamper et al.[5] and Raven, Willi and Rumsby[6] have used Faraday rotation to measure the magnetic fields in laser-produced plasmas at laser irradiances of 10^{15}-10^{16} W/cm^2 and have reported fields of 1-2 megagauss (MG). In those measurements, density gradients limited the distance that the probing light beam could penetrate the plasma to values greater than 100 μm from the target surface.

A comparison of the advantages and disadvantages of Faraday rotation and Zeeman splitting to measure magnetic fields will now be given. Faraday rotation (1) requires an external, polarized light source, (2) also time resolution (typically less than 1 nsec) if the external light source is of short duration, (3) gives information that is the integral of the product of magnetic field and electron density along the optical path of the probe beam, and (4) gives good spatial resolution transverse to the probe beam. On the other hand, Zeeman effect, which produces the splitting and broadening of spectral lines emitted by the plasma, (1) is a passive diagnostic, (2) allows time-resolved measurements (typically a few nsec) to be made, (3) gives the average magnetic field (but not the electron density) along the line of sight, (4) gives moderate spatial resolution of the magnetic field, and (5) with the proper choice of a spectral line allows observations to a higher density region of the plasma than would the Faraday rotation method. Unfortunately, the Zeeman splitting technique requires considerable effort to analyze the spectral line shape, since other broadening mechanisms such as thermal Doppler and Stark broadening as well as instrumental broadening and Doppler shifts due to mass motion are also present.

Peacock and Norton[8] had used the Zeeman effect to measure megagauss magnetic fields in a plasma focus device. For these measurements they chose the helium-like CV $1s2s^3S_1$-$1s2p^3P_{2,1,0}$ multiplet spectral lines which were emitted from their plasma. We have chosen the same multiplet with spectral lines for $J = 2$ at 2270.9 Å, $J = 1$ at 2277.9 Å, and $J = 0$ at 2277.3 Å for the Zeeman splitting measurements described in this report. Reasons for the choice of this multiplet are (1) it is relatively

Manuscript approved July 27, 1983.

insensitive to Stark broadening, since the line is a transition from energy states with low principal quantum numbers, (2) observations could be made in the quartz UV where standard polarization sensitive optics can be used, (3) the spectral line comes from a relatively high temperature (~100 eV) region of the plasma where one expects the magnetic field to be present, and (4) calculation of Zeeman splitting in the intermediate magnetic field region was tractable. LS coupling could be assumed in our calculations of the transition from weak field (anomalous Zeeman effect) to strong field effect (Paschen-Back[9] effect).

Irons, McWhirter and Peacock[10] did extensive spectroscopic investigations of the C^{+4} ions produced by the laser irradiation of polyethylene foils. In these studies, they showed that the C^{+4} ions can be seen up to a centimeter from the target surface, and further, they noted that although the ions primarily are emitted perpendicular to the target surface, there is a radial velocity component (several times smaller than the axial component) parallel to the target surface. Also, Herbst and Grun[11] in a recent study using a novel tracer-dot technique have shown that the fluid flow of ablated plasma from planar target curves away from the target normal with appreciable radial velocity component.

Further, it is shown in this report that when absorption of the spectral line occurs in conjunction with the Zeeman effect, it is possible to measure smaller magnetic fields at a given wavelength resolution than could be measured without absorption.[12] In this study, magnetic fields were measured with field strengths of 200 kilogauss (kG) and below.

II. SPECTRAL LINE BROADENING EFFECTS

A. General Considerations

According to Zeeman effect theory,[13] when a plasma is in a magnetic field, the light emitted perpendicular to the magnetic field lines is linearly polarized with one set of components polarized parallel to the magnetic field (π-components) and the other set of components polarized perpendicular to the magnetic field (σ-components). In this experiment observations will be made perpendicular (as near as possible) to the azimuthal magnetic field lines; by using polarizers the profiles of the spectral lines containing the π-components can be separated from those containing the σ-components. To obtain a measurement of the magnetic field using Zeeman splitting one must address also the other processes that lead to the broadening or wavelength shifting of the spectral lines. Generally, it is necessary to have the width of the Zeeman splitting comparable to or greater than the net broadening from these other processes.

Since the plasma emitting the CV multiplet is a high density, hot plasma one has to consider the broadening of the spectral lines by Stark and thermal Doppler effects. To estimate the broadening of lines by Stark effect, we have used interferometric measurements[14] made under similar conditions to get an estimate of the electron density and then used the following relation for the broadening caused by inelastic and superelastic collisions;[15]

$$\delta\lambda_S = (10^{-8})\frac{\lambda^2}{2\pi c}\left[\frac{4}{3}\right] q_e N_e. \tag{1}$$

Here $\delta\lambda_S$ is the full width at half-intensity in Å, λ is the wavelength of the line in Å, c is the velocity of light, q_e is the excitation rate for the transition $1s2s^3S \rightarrow 1s2p^3P$ (10^{-9} cm^{3}s^{-1}) which was calculated by Blaha,[16] and N_e is the electron density in cm^{-3}. The excitation rate is a weak function of temperature and is found to be dominated by electron collisions. (Should the electron temperature be lower by a factor of 2, the Stark width would increase by no more than 20 percent.) At the time and position of observation in our experiment, the electron density is estimated to be between 10^{19}-10^{20} cm^{-3}. Using these values in Eq. (1), the full width at half-intensity of the Stark broadened line lies between 0.18 and 1.8 Å at an electron temperature of 100 eV.

The thermal Doppler broadening of the spectral lines can be estimated if the ion energies are known. The electron temperature is estimated to be between 80-100 eV, which is the temperature range for maximum emission of the CV lines,[16] and the ion temperature should approximate the electron temperature when the electron densities are this high. The following equation can then be used to calculate the width of a spectral line from thermal Doppler broadening;[17]

$$\delta\lambda_D = 7.16 \times 10^{-7}\lambda(T/M)^{1/2}, \tag{2}$$

where $\delta\lambda_D$ is the full width at half-intensity in Å, T is the ion temperature in keV, λ is the wavelength of the spectral line in Å, and M is the atomic weight. For an estimated ion temperature of 80-100 eV, the thermal width of the CV 2270.9 Å line would fall between 0.44 Å and 0.5 Å. Also, if the instrumental width is known, an estimate of the Stark-Doppler width of the line can be made from the π-profile, which is only weakly sensitive to the magnetic field strength. This estimate, including a correction for opacity effects (described later in this paper), gave a Stark-Doppler width for these conditions of 0.6 Å, which falls between the values derived from the estimated N_e and T_i given above.

In addition to the thermal Doppler width of the spectral line, there is an actual shift of the wavelength of the line due to mass motion. This is due to the radial motion of the plasma plume away from the laser axis. These velocities are about 35% of the axial velocities. Normally, in an optically thin plasma this would give a wavelength shift both to the red and to the blue since the expansion occurs both toward and away from the observer. However, as will be explained later in this report, only the blue-shifted emission is seen because the red-shifted emission has to pass through the dense central region of the plasma plume and is almost completely absorbed. The wavelength shift was measured to be 1.4 Å to the blue. Using the Doppler formula,

$$\frac{\Delta\lambda}{\lambda} = v/c, \tag{3}$$

we find that the mean radial velocity is 1.4-1.8 $\times 10^7$ cm/sec, which is consistent with other measurements.[11] This causes little problem in the interpretation of the data, because all of the lines measured have a constant wavelength shift, which can simply be subtracted from the data.

The instrumental width of the spectrograph was determined by scanning a very narrow spectral line from a Geissler-tube light source. It was found that the spectral line shape was a Gaussian with the full width at half-intensity corresponding to the widths of the entrance and exit slits of the monochromator. Two slit widths, 200 and 100 μm, were used in this study, giving instrumental widths of 1.5 Å and 0.75 Å, respectively. Having some confidence in the shape of the broadened spectral lines, it is now possible to use this data to calculate the shapes of the multiplet for different values of the magnetic field.

First, it is necessary to calculate positions and intensities of the π and σ components of the CV multiplet for the range of magnetic fields that we are considering, i.e., 0-1 MG. Since we are in the *intermediate* magnetic field strength regime, the weak-field approximation cannot be used and a more detailed calculation must be done. This calculation is described in the Appendix. A typical Zeeman pattern for $B = 0.5$ MG is shown in Fig. 1. The scale along the abscissa is in wave numbers and 0 is located at the center of the $J = 2$ ($^3S_1 - {}^3P_2$) line (2270.9 Å). The π components are plotted above the abscissa and the σ components are plotted below the abscissa. Both the position and the relative intensity of each component can be determined from this plot. Immediately, it is noted that there is appreciable asymmetry compared with the weak-field anomalous Zeeman splitting patterns, e.g., note the difference in the π intensities of the $M = 1$ and $M = -1$ components on the two sides of the $J = 2$ line.

From these calculated Zeeman intensity patterns of the components, a calculation can be done which will give the expected shape of the multiplet as viewed in the two polarizations, π and σ. (See Fig. 2.) To do this a small computer code was written in which each individual component of the Zeeman pattern is broadened by the net amount of Stark, thermal Doppler and instrumental broadening (but without opacity effects), and then the individual contributions of all components are added

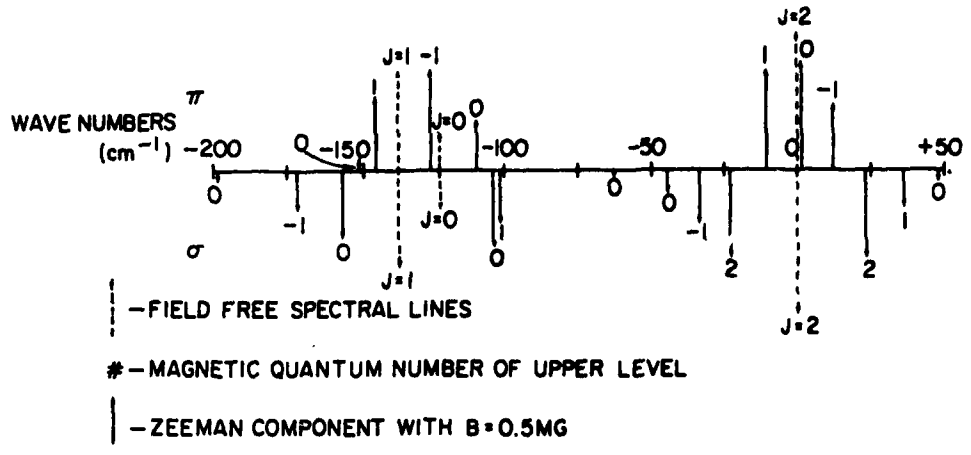

Fig. 1 — Zeeman pattern for the triplet CV $^3S_1 - {}^3P_{2,1,0}$ at $B = 0.5$ MG (50 T)

together to give the emitted optically-thin line spectral shape. These computed lines are then similar in shape to the spectral lines which are actually measured and by choosing the calculated profile which best fits the measured profile one can determine the approximate value of the magnetic field strength.

B. Opacity Corrections

The observed shapes and ratios of the σ to π line intensities suggested that opacity effects were important. It is well known that the absorption coefficient of a spectral line is strongly dependent on the line shape,[19] and at zero magnetic field is a maximum at the center of the spectral line. Thus, the absorption coefficient at the line center will be different for the π and σ profiles in the presence of a magnetic field. This is because the π components peak at the same wavelength as the spectral line at zero magnetic field, whereas the σ components have a dip at the center of the line. When the opacity of the plasma is appreciable, the π components will therefore suffer more absorption than the σ components. This will change the total intensity of the line so that the magnetic field effects become observable at relatively low fields, i.e., even when differences in the optically thin line shapes are still obscured by instrumental broadening. Indeed, the relative amplitudes of the π and σ profiles can be inverted.

Opacity effects in the experiment within the annular emitting region were modelled by setting the opacity of the emitting region ($k_\lambda l$) equal to $C_1 I_t(\lambda)$, where $I_t(\lambda)$ is the total thin-line intensity or line shape. Opacity effects in the cooler, outer region were similarly modelled by setting the opacity of the outer region equal to $C_2 I_t(\lambda)$. The coefficients C_1 and C_2 are adjustable parameters. Since, in the code, the total intensity $I_t(\lambda)$ of all components is separately normalized to unity for the π and σ components, opacity effects will only become dominant when the coefficients are much greater than one. The relation giving the emitted intensity of the line with opacity effects included is,

$$I_e(\lambda) = \frac{1}{C_1}\underbrace{\left[1 - \exp\left[-C_1 I_t(\lambda)\right]\right]}_{\text{Emission Region}} \underbrace{\exp - \left[C_2 I_t(\lambda)\right]}_{\text{Outside Region}}. \tag{4}$$

It was found in matching the data, that the coefficient C_1 for the emitting region was not large compared to one. Also, the opacity correction factor $1 - \exp\left[-C_1 I_t(\lambda)\right]$ for the emitting region was normalized (by dividing by C_1) so that the optically thin intensity $I_t(\lambda)$ is recovered in the limit of small C_1. However, a large value of C_2 (~ 5) was required to match the data; the correction factor $\exp\left[-C_2 I_t(\lambda)\right]$ is the fraction of light transmitted through the cooler absorbing (outer) region. Note that when both regions are optically thin (both C_1, C_2 small), the optically thin emission $I_t(\lambda)$ is recovered. The opacity effect is included in the analysis before the instrument function is convolved with $I_e(\lambda)$ to get $I_e'(\lambda)$, which can then be directly compared with the observed line profiles.

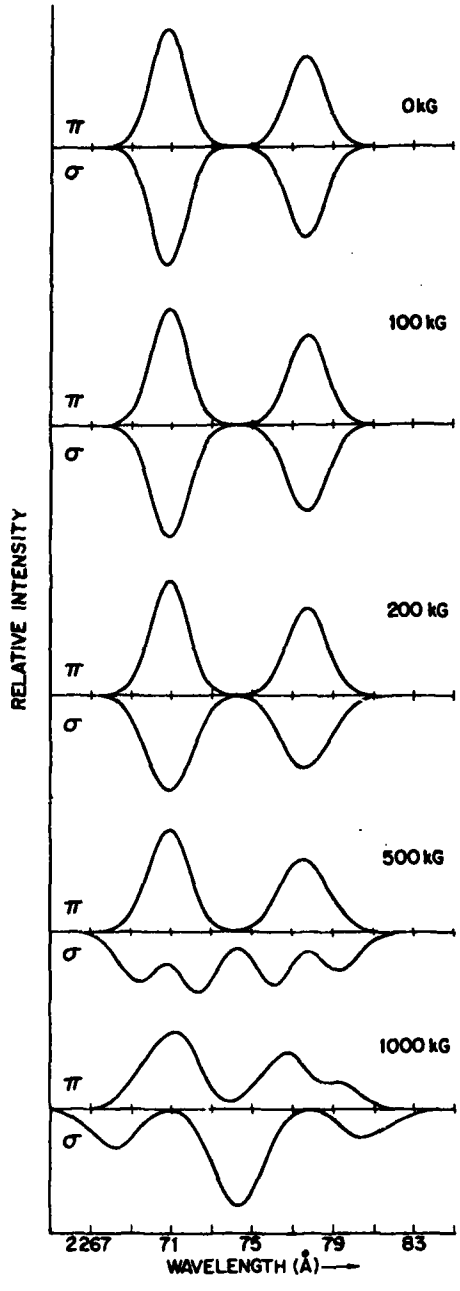

Fig. 2 — Calculated broadened lines including Zeeman splitting of the CV multiplet as a function of magnetic field strength in the range 0-1000 kG. The π profile lines are plotted above the abscissa and the σ profile below the abscissa. Thermal and Stark broadening (1.6 Å) and instrument broadening (0.75 Å) are included in the calculation.

III. EXPERIMENT

In this experiment, a pulsed Nd:phosphate glass laser beam (30-40 J in 5 nsec) at 1.05 μm irradiates a 50-μm thick carbon target in the near field of an f/6 lens. (See Fig. 3a.) In the first set of the measurements a 7-cm diameter mask was placed ahead of the focusing lens so that a ring-shaped laser intensity pattern with an outer diameter of approximately 0.35 mm and a deep minimum would fall onto the target (allowing a larger density gradient and magnetic field to develop). In the second set of measurements the mask was removed from the beam so that a focal-intensity distribution which is almost flat-topped (but with a shallow minimum at the focal spot center) would be incident on the target. The plasma light was collected by an f/1.6 parabolic mirror, M1. The mirror was placed one focal length from the target so that a collimated light beam would be transmitted via plane mirrors, M2, M3, M4 to the f/5 concave mirror M5 which focused the beam through a Wollaston prism onto the slit of a 1-m spectrograph. The collected light always had small angles of incidence with respect to the mirror normals in order to minimize depolarization effects. The magnification of this optical train was 5.3 at the entrance slit of the spectrograph. The optics were aligned so that the image of the spectrograph slit at the center of the plasma plume was parallel to the target surface and 400 μm from the surface. (See Fig. 3b.) (This distance was chosen because a reasonable spectral line-to-continuum ratio could be obtained there. At distances closer to the target surface, the continuum intensity overpowered the line intensities.) The cross-sectional area of the slit image at the center of the plume is $\sim$20 μm (or 40 μm for the 200 μm slit width) by $\sim$200 μm, and emitted light from f/1.6 cones on both sides of the focal region is accepted by the detector.

The Wollaston prism, shown in the side view of Fig. 3a, vertically separated (along the slit) the light beam from the plasma plume into the two orthogonal polarizations, π and σ, so that these polarizations would then continue to be separated in passing through the spectrograph. Mirrors at the exit slit of the spectrograph then directed the two polarized signals into separate photomultiplier tubes. To optimize the intensity collected by the detectors at this wavelength, a spectrograph grating blazed at 2000 Å was used. The signal from the photomultipliers (RCA 1P28) was sent through 50-Ω cables to fast recording oscilloscopes (Tektronix 7104), giving a system time-response of 3 nsec. A relative intensity calibration of the spectrograph and detectors was made using a deuterium arc lamp. Also, the continuum intensity at 2256 Å, which should not be polarized, was used to calibrate on a relative scale the entire optical train. A calibration of the spectrograph wavelength scale was made using a Hg Pen-Ray light source. Using this optical setup the intensities of the π and σ emissions at a particular wavelength are recorded separately and simultaneously. To obtain the spectral line shapes it is necessary to assume shot-to-shot reproducibility and to take a sufficient number of shots to cover the line shape, one small increment of wavelength at a time.

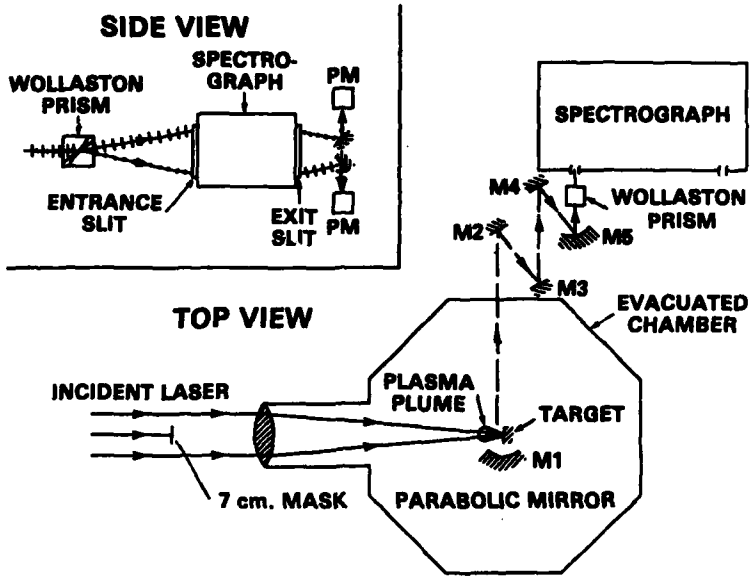

(a)

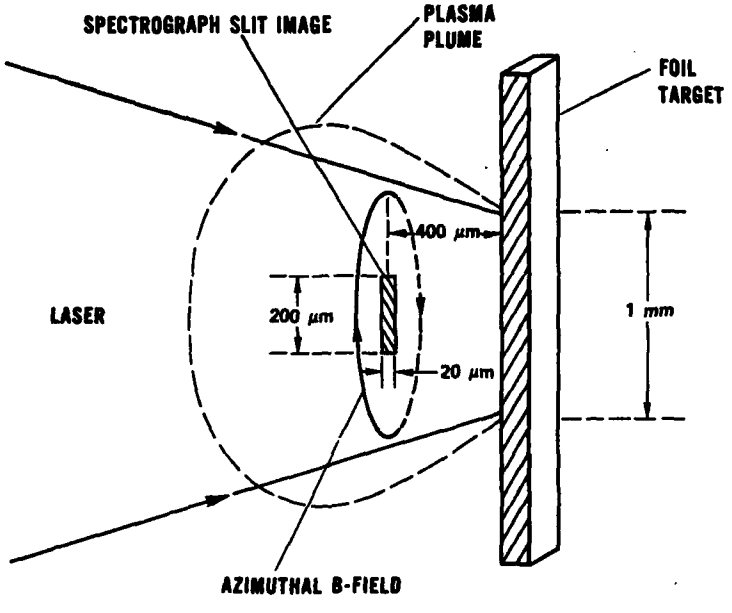

(b)

Fig. 3 — (a) Experimental arrangement (b) Area of observation

IV. RESULTS AND ANALYSIS

A. General

Typical photomultiplier oscillograms are shown in Fig. 4. The two traces shown were taken on the same shot near the peak of one of the CV lines; (a) signal with π-polarization and (b) signal with σ-polarization. Two prominent peaks are seen on each trace. The first peak is due to the early rise of the continuum (and possibly the CV line) intensity. Since the peak temperature that is produced in the plasma plume is greater than 100 eV, e.g., about 200 eV, the CV line initially burns through and does not radiate significantly until the temperature falls later in time; then recombination occurs and the CV line reappears. Thus, the second peak is primarily due to the CV line emission as the plasma temperature decreases to between 80 and 100 eV. (The contribution of the underlying continuum measured on a separate shot, is subtracted off of the signal shown here.) A fiducial signal is fed into the oscilloscope so that the time of the CV signal with respect to the time of the peak of the laser pulse can be determined. Near the spectral line intensity peak, the line-to-continuum ratio is 3 or more.

It is assumed in these studies that the CV (C^{4+}) ions are distributed in a conical annulus about the target normal. This is expected for the case of a ring-shaped focal spot, but is also produced from the intensity distribution with no mask in the beam as well; due to our intensity distribution having a shallow central minimum. Figure 5 shows a cross sectional view of the plasma plume. In this c the interior of the plume is cooler and more dense than the surrounding ring (due to the lower lase ten-sity at the center and the flow of mass from the ring into the central region.)[11,14] Because the ular

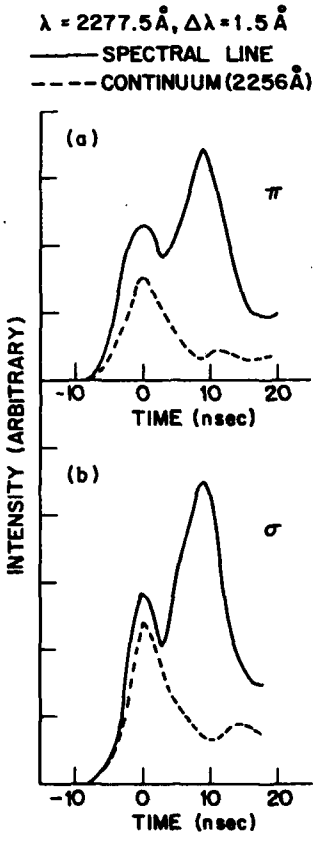

Fig. 4 — Typical photomultiplier oscillograms. The time $t = 0$ corresponds to the time of the peak of the laser pulse.

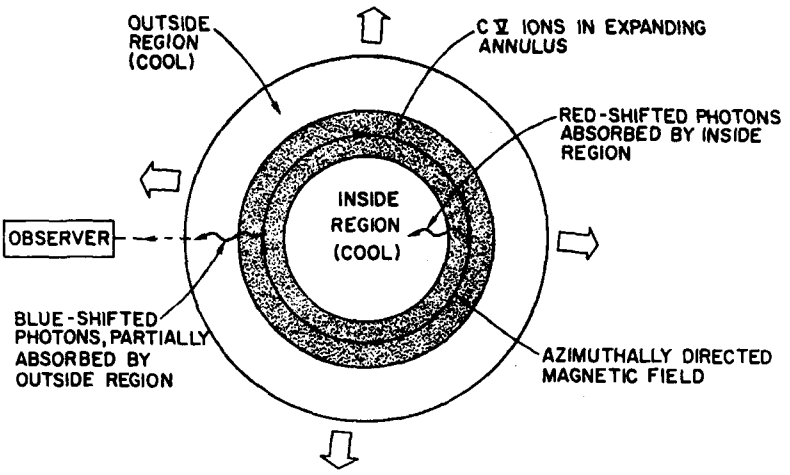

Fig. 5 — Cross-sectional view of plasma plume

ring is expanding away from the center, an observer would see photons produced on the near side of the ring, blue-shifted, and those on the far side of the ring, red-shifted. However, because the center region of the plume is relatively cool, is at a higher density and is large (~mm), the red-shifted photons are absorbed and do not reach the observer. As discussed earlier, the blue-shifted CV lines are also partially absorbed, particularly at later times, by the region outside of the annular region emitting the CV light.

Although the magnetic field is in a clockwise direction in the drawing in Fig. 5, the Zeeman effect cannot distinguish a clockwise from a counterclockwise field. Observations of the line emission are made perpendicular to the laser axis and intersecting the laser axis, so that the observations are approximately perpendicular to the magnetic field.

As mentioned in the introduction, to determine a magnetic field from the line profile measurements, one must assume the composite shape of the Stark and Doppler broadening of the spectral line, use the measured instrumental width, and calculate the Zeeman pattern for the expected range of the magnetic field. If absorption is also present (as is usually the case), this too, will have to be taken into account. Then one can determine the magnetic field which will give the best fit to the lin profile. Since this analysis involves a rather tedious calculation, an interactive computer code was written for this purpose. Our calculation utilized the values of shifts and intensities for intermediate magnetic fields of each π and σ component as described in the Appendix. The steps in the calculation are as follows:

1. First, a Stark-Doppler profile of the individual Zeeman components was assumed. (This decision was guided by estimates of N_e from interferometric measurements and T_e from the CV emission data.)

2. This Stark-Doppler width was then assigned to both the π and σ components of the Zeeman profile for a particular assumed value of the magnetic field. Each component is shifted from its zero field location and its relative amplitude set according to its intermediate field calculation. The profiles of the 3 π components of the $J = 2$ line (or the 6 σ components) are then added together to give a net π (or σ profile); at this point no absorption effects have been included. We now have the optically thin profile $I_t(\lambda)$.

3. Next, the opacity effects are included. This is done for the emitting and outside regions of the plasma by adjusting coefficients C_1 and C_2 and using Eq. (4).

4. Finally, then, to calculate the "observed" line profiles, one must convolve the $I_e(\lambda)$ profile with the known instrument profile. The instrument function used was a Gaussian with a FWHM of 1.5 Å, or 0.75 Å, as appropriate.

5. The computed profile $I'_e(\lambda)$ now can be compared to the measured profile; if it does not fit, a new value of the magnetic field can be tried, a new Stark-Doppler width can be used, or the values of the opacity C_1 and C_2 may be varied to obtain a satisfactory fit.

B. Experiments with a Ring-Shaped Laser Focal Spot

In Fig. 6 a comparison is shown of the experimental profile for the $J = 2$ line of the CV multiplet with a theoretical profile for 200 kilogauss. Since the data for $J = 0$, $J = 1$ lines is incomplete we did not include them in the paper. The experimental profile was observed 5 nanoseconds after the peak of the laser pulse, and near the time of the peak intensity of the $J = 2$ line (centered at 2270.9 Å). The measured data points of the π components are noted with crosses and the data points for the σ components are shown with circles. We assume reproducibility of the plasma plume and take only one or two shots for each wavelength (which gives simultaneous data for both π and σ components). The scatter in the data is indicative of the error in this procedure. Generally, the data points fall within a scatter bracket of ±20%; however, at +3 Å the scatter is higher. (This is possibly due to the fact that the $J = 0$ line is beginning to overlap the $J = 2$ line at that wavelength.) For the fit shown here, rather small opacity parameters $C_1 = 0.3$ and $C_2 = 2$ are required. The agreement in profile fits was better at 200 kG than at 100 kG or 300 kG, although it was noted that a slightly smaller π width would agree better with the data, indicating that a field slightly larger than 200 kG would agree somewhat better with the data.

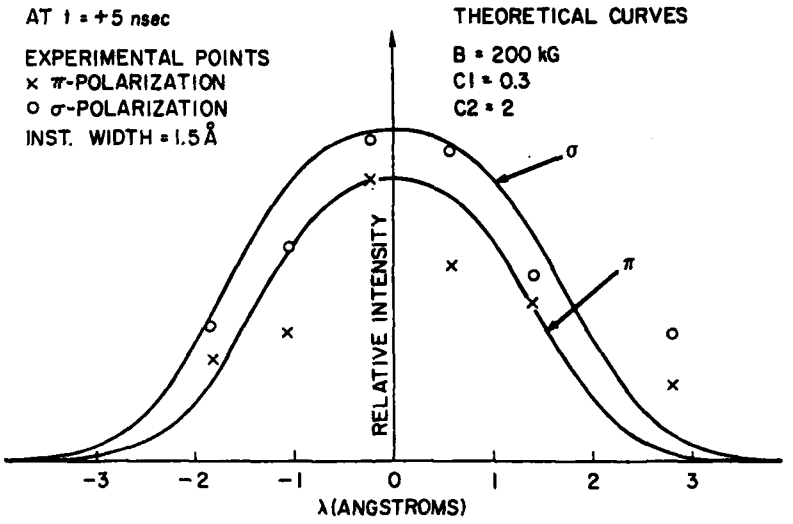

Fig. 6 — Comparison of experimental data and calculated profiles for $J = 2$ line at $t = 5$ nsec for ring-shaped laser focal spot. Measured data points: X are for π polarization and 0 are for σ polarization. Curves are calculated using an instrument width = 1.5 Å, the Stark-Doppler width = 1.44 Å, and $B = 200$ kG.

Data was also analyzed at a later time (8 nsec after the peak of the laser pulse) on these same shots. The profile obtained at this time is shown in Fig. 7a. The striking feature in this data is that the σ line is nearly twice as intense as the π line at the center of the profiles. It was found that by making the surrounding region more absorbing ($C_2 = 5$) and continuing to assume a magnetic field of 200 kG the theoretical curve gives a fairly good fit to the experimental data. A slightly smaller σ width would give an even better fit to the data, indicating that the field is just under 200 kG. The important point to be made regarding this data is that the only way the σ profile could have a much higher intensity than the π profile is for *absorption* to be taking place, in which the σ profile in the presence of a magnetic field has a dip in the line center (where peak absorption would normally occur) and therefore, has less absorption than the π-profile which has a sharp peak at the line center even with a magnetic field.

1. Error Analysis

We have several free parameters which can be varied to get a fit to the experimental data. Since we do not have precise auxiliary data to pin down these variables, it is necessary to do trial calculations varying the parameters individually to see if we can get a satisfactory fit with different sets of values of the parameters, i.e., to see if we have a unique fit with the values chosen. For this set of calculations, the value of B was varied between 0 and 300 kG, C_1 was varied from 0.3 to 7, C_2 was varied from 0.1 to 10, and the Stark-Doppler width ($W_{S\text{-}D}$) was varied from 0.36 Å to 1.5 Å (where the upper limit could be determined by the width of the π component, whose width is much less dependent on the magnetic field than the σ component).

From over 40 calculations, we found that the best fit occurred with $W_{S\text{-}D} = 0.6$ Å, $C_1 = 0.3$, $C_2 = 5$, and the magnetic field = 200 kG. An example of the sensitivity of the line shape to the magnetic field, holding the other variables constant to the values given above is shown in Fig. 7b and 7c. (All of the curves are normalized with respect to the σ values at 0 Å.) It is noted in Fig. 7b where $B = 0$ G that the π and σ curves are identical, and thus could not fit the data. The data points are also plotted on the same set of curves in Fig. 7c. It is seen that the best overall fit of the calculated curves with the data points, considering both the amplitude and the shape is given by the 200 kG σ and π curves. (A somewhat better fit might be obtained if increments of magnetic field smaller than 100 kG were used.) From this error analysis, it is concluded that the accuracy for the magnetic field measurement is ± 75 kG when absorption is present.

C. Experiments with a Flat-topped Focal Spot (Mask Removed from Laser Beam)

When the mask in front of the lens is removed, the focal intensity distribution is relatively flat-topped with a shallow minimum at the center. The diameter of the focal spot was 0.48 mm, which contained 90% of absorbed laser energy. The resulting CV data is shown in Fig. 8. The instrumental width remained 1.5 Å, the same as for the previous data. The theoretical curve for $B = 100$ kG, $C_1 = .01$, $C_2 = 3.5$ and the Stark-Doppler width of 1.5 Å fits the experimental data for the $J = 2$ line fairly well in both shape and amplitude for both the π and the σ lines. Due to the lack of structure in the σ line, it appeared desirable to have better wavelength resolution. For this reason another data run was taken in which the instrumental width was decreased from 1.5 Å to 0.75 Å, the other experimental conditions remaining approximately the same.

The results with the improved wavelength resolution are shown in Fig. 9; more structure can be seen in the profiles. For the $J = 2$ line both the π and the σ lines are in good agreement, in shape and amplitude, with the calculated curve. (The Stark-Doppler broadening parameter was changed from 1.5 Å to 1.0 Å and the opacity parameters were changed from $C_1 = .01$ to 0.3 and $C_2 = 3.5$ to 3.0 from those used in Fig. 8 since the wavelength resolution is better here and more accurate values of the above parameters can be chosen.) Again these curves have been plotted for different values for B to show the sensitivity of the technique. The best fit was again $B = 100^{+75}_{-100}$ kG.

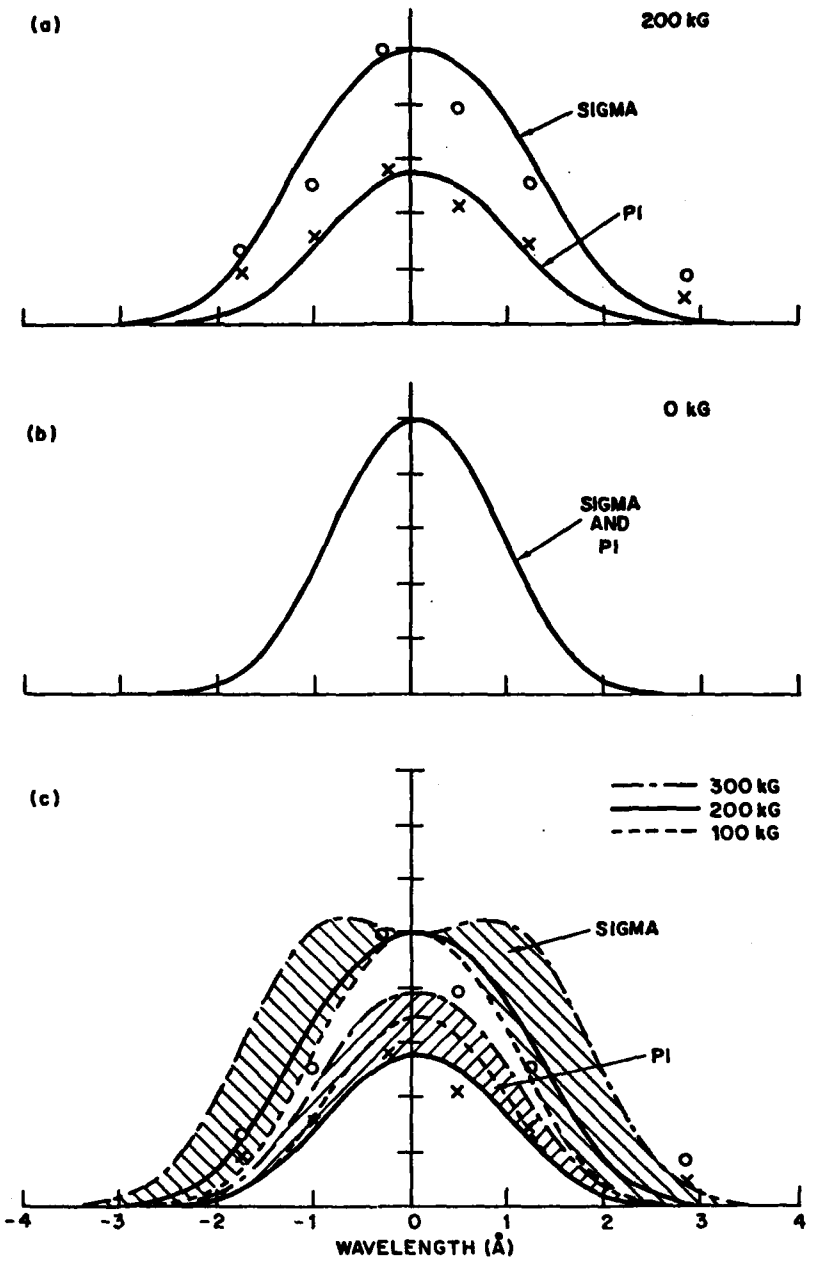

Fig. 7 — Comparison of measured data and calculated profile for $J = 2$ line at $t = 8$ nsec for the same data runs as used for Fig. 6. Measure data points: X are for π polarization and 0 are for σ polarization. Curves are calculated using an instrumental width = 1.5 Å, the Stark-Doppler width = 0.6 Å and the B varied between 0 and 300 kG. (a) $B = 200$ kG, (b) $B = 0$ G, (c) B varied between 100 kG and 300 kG to show error spread in data.

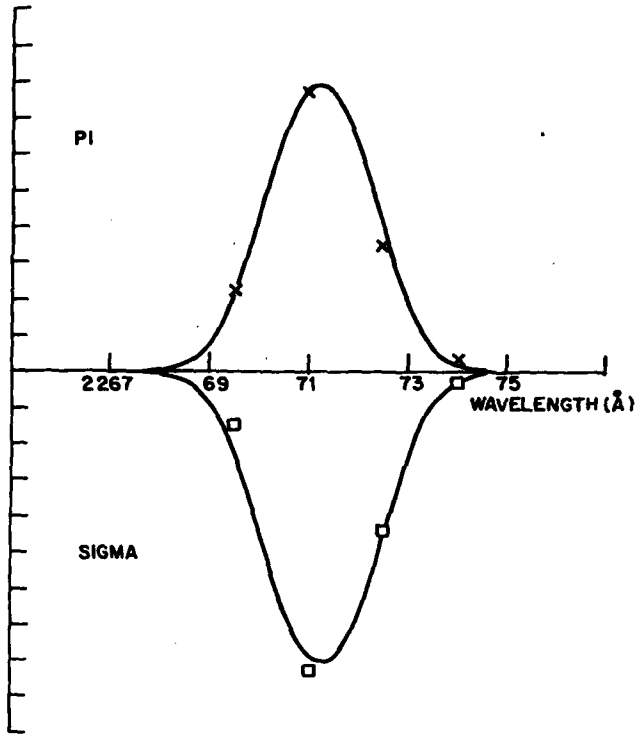

Fig. 8 — Comparison of measured and calculated profiles for the $J = 2$ line at $t = 8$ ns for standard focal spot (mask removed from laser beam). The π line is plotted above the abscissa and the σ line is plotted below the abscissa. The data points are measured points and the curves are calculated, using an instrument width of 1.5 Å, a Stark-Doppler width of 1.5 Å, and $B = 100$ kG.

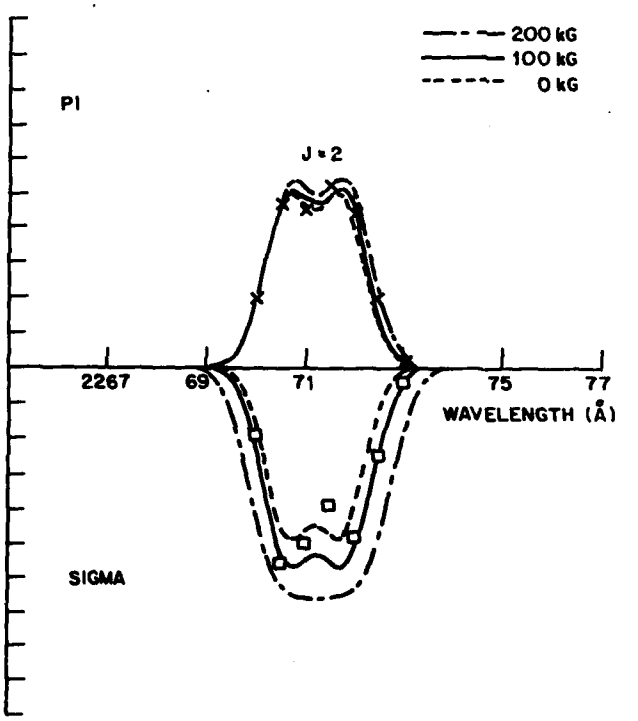

Fig. 9 — Comparison of measured data points and calculated profiles for the $J = 2$ line at $t = 9$ ns for standard laser focal spot. The π line is plotted above and the σ line below the abscissa, which is the wavelength in Angstroms. The curves are calculated using an instrument width of 0.75 Å, a Stark-Doppler width of 1 Å, and the magnetic field values of 0, 100, and 200 kG.

V. DISCUSSION AND CONCLUSIONS

The magnetic field produced when a pulsed laser beam is focused onto a target is measured for the first time using the Zeeman effect. These measurements, which were made at electron densities of $10^{19} - 10^{20}$ cm^{-3}, allowed somewhat lower magnetic fields ($\sim$100 kG) to be measured than the Faraday Rotation technique, and further did not require the measurement of the electron density.

The plasma opacity present enhanced the accuracy of the *B*-field measurement. At laser irradiance of $\sim 10^{12}$ W/cm^2, the magnetic field increased from 100 kG to 200 kG when the focal spot was changed from a flat-topped distribution to a ring pattern, which caused higher density gradients. The magnetic field measured using the Zeeman effect with the ring shaped focal spot is consistent with a Faraday Rotation measurement made under similar conditions.

In summary, magnetic fields of 1-2 MG were seen previously when the laser irradiance was high ($\sim 10^{16}$ W/cm^2) and pulse duration short (100 psec); here the magnetic field was found to be reduced to 200 kG and below for lower irradiances (5×10^{12} W/cm^2), longer pulse durations (3-4 nsec) and later observation times (5-8 nsec).

ACKNOWLEDGMENTS

The authors would like to acknowledge discussions and the support of S. Bodner and valued advice and assistance of S. P. Obenschain, J. Grun, M. J. Herbst, R. R. Whitlock, and F. Young. The technical assistance of N. Nocerino, E. Turbyfill, M. Fink and B. Sands is greatly appreciated.

This work was supported by the Department of Energy and the Defense Nuclear Agency.

Appendix
THEORY AND CALCULATION OF ZEEMAN EFFECT FOR INTERMEDIATE FIELDS

The field-free $(1s2p)^3P_J$ levels of CV for $J = 0$, 1 and 2 are rather closely spaced, with intervals[20] $E_2(0) - E_1(0) = 136\ \text{cm}^{-1}$ and $E_1(0) - E_0(0) = -13\ \text{cm}^{-1}$. Because of the small (and inverted) interval between the $J = 1$ and 0 levels, use of lowest order perturbation theory for the Zeeman effect as in Ref. 8 would not be justified for the field-strengths of interest. This is easily seen by comparing the magnitude of magnetic interactions,[21]

$$|H_{\text{mag}}| \approx \mu_o B = 46.686\ B\ \text{cm}^{-1}, \tag{A1}$$

with B in megagauss, with the above field-free intervals. Particularly important[21] here are the changes in relative intensities, relative to the low field (anomalous Zeeman effect) results, of the various Zeeman components associated with the $2^3P_J - 2^3S_1$ transitions observed in our experiment.

To obtain a quantitative theory of the Zeeman effect for intermediate fields, one writes the 2^3P eigen functions as superpositions of LS eigen functions of various $J \geqslant |M|$,

$$|LSM\rangle = \sum_{J \geqslant |M|} C_{JM} |LSJM\rangle \tag{A2}$$

Only the magnetic quantum numbers M remain "good," and the expansion coefficients C_{JM} follow from the Schrödinger equations

$$[H_J(0) + H_{\text{mag}}]|LSM\rangle = E_{J'M}(B)|LSM\rangle \tag{A3a}$$

where $H_J(0)$ is the field-free Hamiltonian with eigenvalues $E_J(0)$ and eigenfunctions $|LSJM\rangle$. The nonvanishing matrix elements of the magnetic interaction are in the $|LSJM\rangle$ representation[22]

$$\langle 11\,JM|H_{\text{mag}}|11\,JM\rangle = \frac{3}{2} M\mu_o B, \tag{A4a}$$

$$\langle 11\,JM|H_{\text{mag}}|11\,(J-1)M\rangle = -\frac{1}{2}\mu_o B \left[\frac{(J^2 - M^2)(9 - J^2)}{4J^2 - 1}\right]^{1/2} \tag{A4b}$$

for diagonal and off-diagonal elements, respectively. According to the various properties of $H_J(0)$, H_{mag}, and $|LSJM\rangle$, the system of equations corresponding to Eq. (A3a) becomes for each M a set of coupled linear equations

$$\sum_{J=J''-1,J'',J''+1} \{[E_{J''}(0) - E_{J'M}(B)]\delta_{J''J} + \langle J''M|H_{\text{mag}}|JM\rangle\} C^{J'}_{JM}(B) = 0. \tag{A3b}$$

which can only be solved if the level energy $E_{J'M}(B)$ is such that the determinant of the matrix in curly brackets vanishes. For each such root, J', one then finds the coefficient vector $C^{J'}_{JM}(B)$ which will be assumed to be normalized. The actual matrices are

$$\left\{\ \right\} = \begin{vmatrix} [E_2(0) - E_{J'M}(B)] & -\frac{1}{\sqrt{3}}\mu_o B & 0 \\ -\frac{1}{\sqrt{3}}\mu_o B & [E_1(0) - E_{J'M}(B)] & -\sqrt{\frac{2}{3}}\mu_0 B \\ 0 & \frac{-\sqrt{2}}{3}\mu_o B & [E_o(0) - E_{J'M}(B)] \end{vmatrix}$$

$$\left\{\ \right\} = \begin{vmatrix} [E_2(0) \pm \frac{3}{2}\mu_o B - E_{J'M}(B)] & -\frac{1}{2}\mu_o B \\ -\frac{1}{2}\mu_o B & [E_1(0) \pm \frac{3}{2}\mu_o B - E_{J'M}(B)] \end{vmatrix} \tag{A5}$$

$$\left\{\ \right\} = [E_2(0) \pm 3\mu_o B - E_{J'M}]$$

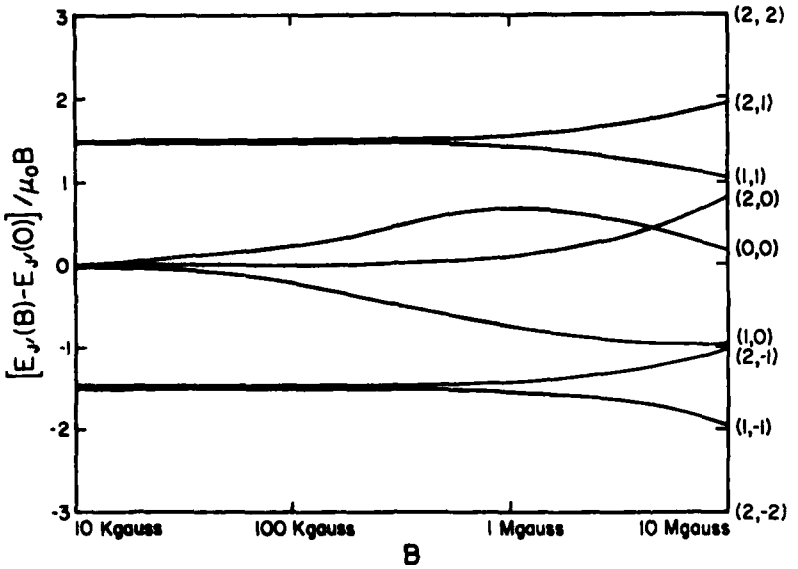

Fig. 10 — Zeeman shifts of (J',M') magnetic sub-levels of 2^3P_J in units of $g = 1$ and magnetic perturbation energy $\mu_o B = 46.686\ \text{cm}^{-1}\ B(\text{MG})$. To obtain the actual level positions, e.g., relative to the zero-field $J' = 2$ level, 123 cm^{-1} and 136 cm^{-1} must be subtracted from the $J' = 0$ and $J' = 1$ Zeeman shifts. This procedure causes the (0,0) level to stay below the (2,0) level for all field values, i.e., there is no crossing of levels.

for $M = 0$, $M = \pm 1$ and $M = \pm 2$, respectively, written in the order of decreasing indices J and J''. It is convenient to refer all energies in the numerical calculations to the unshifted position of the $J = 2$ level, i.e., to use $E_2(0) = 0$, $E_1(0) = -136\ \text{cm}^{-1}$ and $E_0(0) = -123\ \text{cm}^{-3}$. The value of $\mu_o B$ is as in Eq. (A1).

In Fig. 10, the differences of the eigenvalues $E_{J'M}(B)$ and $E_{J'M}(0)$ are plotted, in units of $\mu_o B$, and it is seen that significant deviations from the weak field limit occur for $B > 0.1$ MG. (Note that there is no real level crossing of the (0,0) and (2,0) levels near 5 MG.) The relative intensities of the Zeeman components for observation perpendicular to the field can be calculated from[21]

$$M \to M\colon S_\pi^{J'} = \left| \sum_J C_{JM}^{J'} (-1)^{J-M} \begin{pmatrix} J & 1 & 1 \\ -M & 0 & M \end{pmatrix} [3(2J+1)]^{1/2} \begin{Bmatrix} 1 & 1 & J \\ 1 & 1 & 0 \end{Bmatrix} \right|^2 \tag{A6a}$$

$$M \to M \pm 1\colon S_\sigma^{J'} = \frac{1}{2} \left| \sum_J C_{JM}^{J'} (-1)^{J-M} \begin{pmatrix} J & 1 & 1 \\ -M & \mp 1 & M \pm 1 \end{pmatrix} [3(2J+1)]^{1/2} \begin{Bmatrix} 1 & 1 & J \\ 1 & 1 & 0 \end{Bmatrix} \right|^2, \tag{A6b}$$

where the expressions in large parentheses and large curly brackets are Wigner's $3-j$ and $6-j$ symbols, respectively. The $6-j$ symbols have the values 1/3, −1/3 and 1/3 for $J = 0$, 1 and 2. They may therefore be combined with the phase factors into a common factor 1/3. Using tabulated[21] $3-j$ symbols one obtains for π-polarization

$$M = M' = 0\colon S_\pi^{J'} = \left| \frac{\sqrt{2}}{3} C_{20}^{J'} - \frac{1}{3} C_{00}^{J'} \right|^2 \tag{A7a}$$

$$M = M' = \pm 1\colon S_\pi^{J'} = \frac{1}{6} |C_{\pm 1}^{J'} \mp C_{\pm 1}^{J'}|^2 \tag{A7b}$$

$$M = M' = \pm 2\colon S_\pi^{J'} = 0 \tag{A7c}$$

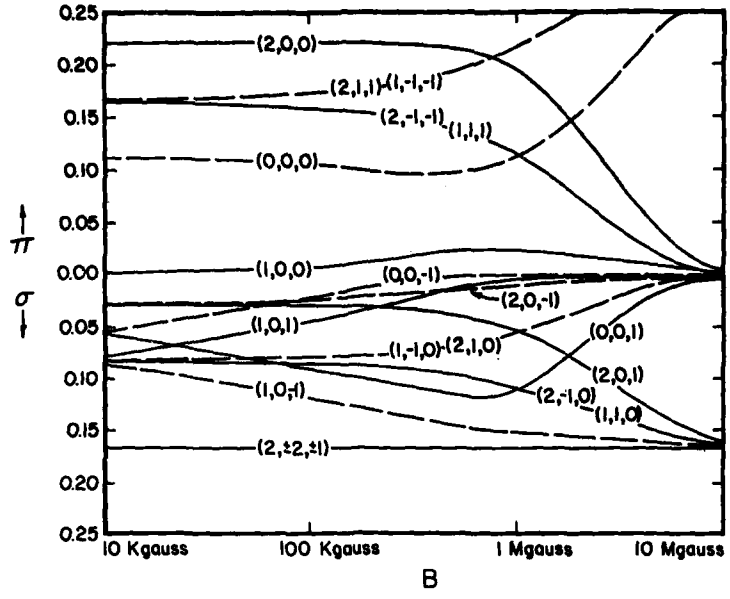

Fig. 11 — Relative intensities of π (up) and σ (down) Zeeman components (J',M',M) of the $2^3P_J1 - 2^3S_1$ transitions as functions of magnetic field strength. Observation is assumed to be perpendicular to the magnetic field.

and for σ polarization

$$M = 0,\ M' = \pm 1\text{: } S_\sigma^{J'} = \frac{1}{18}\left|\frac{1}{\sqrt{2}}\, C_{20}^{J'} \mp \frac{\sqrt{3}}{2}\, C_{10}^{J'} + C_{00}^{J'}\right|^2 \tag{A8a}$$

$$M = \pm 1,\ M' = 0\text{: } S_\sigma^{J'} = \frac{1}{12}|C_{1\pm1}^{J'} \pm C_{1\pm1}^{J'}|^2 \tag{A8b}$$

$$M = \pm 2,\ M' = \pm 1\text{: } S_\sigma^{J'} = \frac{1}{6}|C_{2\pm2}^{J'}|^2 = \frac{1}{6}, \tag{A8c}$$

where M' is the magnetic quantum number of the 2^3S_1 (lower) state. The calculated intensities are shown in Fig. 11. They clearly deviate from the weak field limit already at fields below 0.1 MG.

To compute line rather than level shifts, the shifts of the lower level, namely

$$E_{lM'} = 2M'\mu_o B = 93.372\ M'B\ \text{cm}^{-1} \tag{A9}$$

must be subtracted and the zero-field $2^3P_2 - 2^3S_1$ interval be added. Or, if wavelengths are desired, one calculates the wavelength shifts according to

$$\Delta\lambda_{MM'}^{J'} = -\lambda_J^2[E_{J'M}(B) - E_{J'}(0) - E_{lM'}(B)] \tag{A10}$$

with $\lambda_2 = 2270.9$, $\lambda_1 = 2277.9$ and $\lambda_0 = 2277.3$ Å.

REFERENCES

1. J.A. Stamper, K. Papadopoulos, R.N. Sudan, S.O. Dean, E.A. McLean, and J.M. Dawson, Phys. Rev. Lett. **26**, 1012 (1971); J.A. Stamper, "A Perspective on Self-Generated Magnetic Fields," Naval Research Laboratory Memorandum Report 3872, October 27, 1978.

2. See for example, J.B. Chase, J.M. LeBlanc, and J.R. Wilson, Phys. Fluids **16**, 1142 (1973); N.K. Winsor and D.A. Tidman, Phys. Rev. Lett. **31**, 1044 (1973); W.C. Mead, R.A. Haas, W.L. Kruer, D.W. Phillion, H.N. Kornblum, J.D. Lindl, D.R. MacQuigg, and V.C. Rupert, Phys. Rev. Lett. **37**, 489 (1976).

3. D.W. Forslund and J.V. Brackbill, Phys. Rev. Lett. **48**, 1614 (1982).

4. R.S. Bird, L.L. McKee, F. Schwirzke, and A.W. Cooper, Phys. Rev. A **7**, 1328 (1973); M.G. Drouet and R. Bolton, Phys. Rev. Lett. **36**, 591 (1976).

5. J.A. Stamper and B.H. Ripin, Phys. Rev. Lett. **34**, 138 (1975); J.A. Stamper, E.A. McLean, and B.H. Ripin, Phys. Rev. **40**, 1177 (1978).

6. A. Raven, O. Willi, and P.T. Rumsby, Phys. Rev. Lett. **41**, 554 (1978).

7. Y. Sakagami, H. Kawakami, J. Nagao, and C. Yamanaka, Phys. Rev. Lett. **42**, 839 (1979).

8. N.J. Peacock and B.A. Norton, Phys. Rev. A **11**, 2142 (1975).

9. F. Paschen and E. Back, Ann. Physik **39**, 897 (1912); **40**, 960 (1913).

10. F.E. Irons, R.W.P. McWhirter, and N.J. Peacock, J. Phy. B: Atom. Molec. Phys. **5**, 1975 (1972).

11. M.J. Herbst and J. Grun, Phys. Fluids **24**, 1917 (1981).

12. K.H. Finken, J. Quant. Spectrosc. Radiat. Transfer **22**, 397 (1979).

13. See for example, P. Zeeman, Phil. Mag. **5**, 43, 226 (1897); R.D. Cowan, "The Theory of Atomic Structure and Spectra," (University of California Press, Berkeley, 1981).

14. J.A. Stamper, E.A. McLean, S.P. Obenschain, H.R. Griem, C.K. Manka, D.W. Droemer, and M.J. Herbst, "Generation of Enhanced-Scalelength Plasmas, and Zeeman Study of Magnetic Fields," Naval Research Laboratory Memorandum Report No. 4898 (March 31, 1983).

15. H.R. Griem, "Plasma Spectroscopy," (McGraw-Hill Book Company, New York, 1964).

16. Private communication with Mihan Blaha.

17. V.L. Jacobs, J. Davis, G.E. Rogerson, and M. Blaha, J. Quant. Spectrosc. Radiat. Transfer **19**, 591 (1978).

18. L.H. Aller, "Astrophysics—The Atmospheres of the Sun and Stars," 2nd edition (Ronald Press Company, New York, 1963), p. 111.

19. A.C.G. Mitchell and M.W. Zemansky, "Resonance Radiation and Excited Atoms," (Cambridge at the University Press, 1971).

20. C.E. Moore, Atomic Energy Levels, Vol. 1, NSRDS-NBS 35, U.S. Govt. Printing Office, Washington, DC (1971).

21. R.D. Cowan, ibid.

DISTRIBUTION LIST

DEPARTMENT OF DEFENSE

ASSISTANT SECRETARY OF DEFENSE
COMM, CMD, CONT 7 INTELL
WASHINGTON, D.C. 20301

DIRECTOR
COMMAND CONTROL TECHNICAL CENTER
PENTAGON RM BE 685
WASHINGTON, D.C. 20301
01CY ATTN C-650
01CY ATTN C-312 R. MASON

DIRECTOR
DEFENSE ADVANCED RSCH PROJ AGENCY
ARCHITECT BUILDING
1400 WILSON BLVD.
ARLINGTON, VA. 22209
01CY ATTN NUCLEAR MONITORING RESEARCH
01CY ATTN STRATEGIC TECH OFFICE

DEFENSE COMMUNICATION ENGINEER CENTER
1860 WIEHLE AVENUE
RESTON, VA. 22090
01CY ATTN CODE R410
01CY ATTN CODE R812

DEFENSE TECHNICAL INFORMATION CENTER
CAMERON STATION
ALEXANDRIA, VA. 22314
02CY

DIRECTOR
DEFENSE NUCLEAR AGENCY
WASHINGTON, D.C. 20305
01CY ATTN STVL
04CY ATTN TITL
01CY ATTN DDST
03CY ATTN RAAE

COMMANDER
FIELD COMMAND
DEFENSE NUCLEAR AGENCY
KIRTLAND, AFB, NM 87115
01CY ATTN FCPR

DIRECTOR
INTERSERVICE NUCLEAR WEAPONS SCHOOL
KIRTLAND AFB, NM 87115
01CY ATTN DOCUMENT CONTROL

JOINT CHIEFS OF STAFF
WASHINGTON, D.C. 20301
01CY ATTN J-3 WWMCCS EVALUATION OFFICE

DIRECTOR
JOINT STRAT TGT PLANNING STAFF
OFFUTT AFB
OMAHA, NB 68113
01CY ATTN JLTW-2
01CY ATTN JPST G. GOETZ

CHIEF
LIVERMORE DIVISION FLD COMMAND DNA
DEPARTMENT OF DEFENSE
LAWRENCE LIVERMORE LABORATORY
P.O. BOX 808
LIVERMORE, CA 94550
01CY ATTN FCPRL

COMMANDANT
NATO SCHOOL (SHAPE)
APO NEW YORK 09172
01CY ATTN U.S. DOCUMENTS OFFICER

UNDER SECY OF DEF FOR RSCH & ENGRG
DEPARTMENT OF DEFENSE
WASHINGTON, D.C. 20301
01CY ATTN STRATEGIC & SPACE SYSTEMS (OS)

WWMCCS SYSTEM ENGINEERING ORG
WASHINGTON, D.C. 20305
01CY ATTN R. CRAWFORD

COMMANDER/DIRECTOR
ATMOSPHERIC SCIENCES LABORATORY
U.S. ARMY ELECTRONICS COMMAND
WHITE SANDS MISSILE RANGE, NM 88002
01CY ATTN DELAS-EO F. NILES

DIRECTOR
BMD ADVANCED TECH CTR
HUNTSVILLE OFFICE
P.O. BOX 1500
HUNTSVILLE, AL 35807
01CY ATTN ATC-T MELVIN T. CAPPS
01CY ATTN ATC-O W. DAVIES
01CY ATTN ATC-R DON RUSS

PROGRAM MANAGER
BMD PROGRAM OFFICE
5001 EISENHOWER AVENUE
ALEXANDRIA, VA 22333
01CY ATTN DACS-BMT J. SHEA

CHIEF C-E- SERVICES DIVISION
U.S. ARMY COMMUNICATIONS CMD
PENTAGON RM 1B269
WASHINGTON, D.C. 20310
01CY ATTN C- E-SERVICES DIVISION

COMMANDER
FRADCOM TECHNICAL SUPPORT ACTIVITY
DEPARTMENT OF THE ARMY
FORT MONMOUTH, N.J. 07703
01CY ATTN DRSEL-NL-RD H. BENNET
01CY ATTN DRSEL-PL-ENV H. BOMKE
01CY ATTN J.E. QUIGLEY

COMMANDER
U.S. ARMY COMM-ELEC ENGRG INSTAL AGY
FT. HUACHUCA, AZ 85613
01CY ATTN CCC-EMEO GEORGE LANE

COMMANDER
U.S. ARMY FOREIGN SCIENCE & TECH CTR
220 7TH STREET, NE
CHARLOTTESVILLE, VA 22901
01CY ATTN DRXST-SD

COMMANDER
U.S. ARMY MATERIAL DEV & READINESS CMD
5001 EISENHOWER AVENUE
ALEXANDRIA, VA 22333
01CY ATTN DRCLDC J.A. BENDER

COMMANDER
U.S. ARMY NUCLEAR AND CHEMICAL AGENCY
7500 BACKLICK ROAD
BLDG 2073
SPRINGFIELD, VA 22150
01CY ATTN LIBRARY

DIRECTOR
U.S. ARMY BALLISTIC RESEARCH LABORATORY
ABERDEEN PROVING GROUND, MD 21005
01CY ATTN TECH LIBRARY EDWARD BAICY

COMMANDER
U.S. ARMY SATCOM AGENCY
FT. MONMOUTH, NJ 07703
01CY ATTN DOCUMENT CONTROL

COMMANDER
U.S. ARMY MISSILE INTELLIGENCE AGENCY
REDSTONE ARSENAL, AL 35809
01CY ATTN JIM GAMBLE

DIRECTOR
U.S. ARMY TRADOC SYSTEMS ANALYSIS ACTIVITY
WHITE SANDS MISSILE RANGE, NM 88002
01CY ATTN ATAA-SA
01CY ATTN TCC/F. PAYAN JR.
01CY ATTN ATTA-TAC LTC J. HESSE

COMMANDER
NAVAL ELECTRONIC SYSTEMS COMMAND
WASHINGTON, D.C. 20360
01CY ATTN NAVALEX 034 T. HUGHES
01CY ATTN PME 117
01CY ATTN PME 117-T
01CY ATTN CODE 5011

COMMANDING OFFICER
NAVAL INTELLIGENCE SUPPORT CTR
4301 SUITLAND ROAD, BLDG. 5
WASHINGTON, D.C. 20390
01CY ATTN MR. DUBBIN STIC 12
01CY ATTN NISC-50
01CY ATTN CODE 5404 J. GALET

COMMANDER
NAVAL OCCEAN SYSTEMS CENTER
SAN DIEGO, CA 92152
01CY ATTN J. FERGUSON

NAVAL RESEARCH LABORATORY
WASHINGTON, D.C. 20375
01CY ATTN CODE 4700 S. L. Ossakow
26 CYS IF UNCLASS. 1 CY IF CLASS)
01CY ATTN CODE 4701 I Vitkovitsky
01CY ATTN CODE 4780 J. Huba (10
CYS IF UNCLASS, 1 CY IF CLASS)
01CY ATTN CODE 7500
01CY ATTN CODE 7550
01CY ATTN CODE 7580
01CY ATTN CODE 7551
01CY ATTN CODE 7555
01CY ATTN CODE 4730 E. MCLEAN
01CY ATTN CODE 4108
01CY ATTN CODE 4730 B. RIPIN
20CY ATTN CODE 2628

COMMANDER
NAVAL SEA SYSTEMS COMMAND
WASHINGTON, D.C. 20362
01CY ATTN CAPT R. PITKIN

COMMANDER
NAVAL SPACE SURVEILLANCE SYSTEM
DAHLGREN, VA 22448
01CY ATTN CAPT J.H. BURTON

OFFICER-IN-CHARGE
NAVAL SURFACE WEAPONS CENTER
WHITE OAK, SILVER SPRING, MD 20910
01CY ATTN CODE F31

DIRECTOR
STRATEGIC SYSTEMS PROJECT OFFICE
DEPARTMENT OF THE NAVY
WASHINGTON, D.C. 20376
01CY ATTN NSP-2141
01CY ATTN NSSP-2722 FRED WIMBERLY

COMMANDER
NAVAL SURFACE WEAPONS CENTER
DAHLGREN LABORATORY
DAHLGREN, VA 22448
01CY ATTN CODE DF-14 R. BUTLER

OFFICER OF NAVAL RESEARCH
ARLINGTON, VA 22217
01CY ATTN CODE 465
01CY ATTN CODE 461
01CY ATTN CODE 402
01CY ATTN CODE 420
01CY ATTN CODE 421

COMMANDER
AEROSPACE DEFENSE COMMAND/DC
DEPARTMENT OF THE AIR FORCE
ENT AFB, CO 80912
01CY ATTN DC MR. LONG

COMMANDER
AEROSPACE DEFENSE COMMAND/XPD
DEPARTMENT OF THE AIR FORCE
ENT AFB, CO 80912
01CY ATTN XPDQQ
01CY ATTN XP

AIR FORCE GEOPHYSICS LABORATORY
HANSCOM AFB, MA 01731
01CY ATTN OPR HAROLD GARDNER
01CY ATTN LKB KENNETH S.W. CHAMPION
01CY ATTN OPR ALVA T. STAIR
01CY ATTN PHD JURGEN BUCHAU
01CY ATTN PHD JOHN P. MULLEN

AF WEAPONS LABORATORY
KIRTLAND AFT, NM 87117
01CY ATTN SUL
01CY ATTN CA ARTHUR H. GUENTHER
01CY ATTN NTYCE 1LT. G. KRAJEI

AFTAC
PATRICK AFB, FL 32925
01CY ATTN TF/MAJ WILEY
01CY ATTN TN

AIR FORCE AVIONICS LABORATORY
WRIGHT-PATTERSON AFB, OH 45433
01CY ATTN AAD WADE HUNT
01CY ATTN AAD ALLEN JOHNSON

DEPUTY CHIEF OF STAFF
RESEARCH, DEVELOPMENT, & ACQ
DEPARTMENT OF THE AIR FORCE
WASHINGTON, D.C. 20330
01CY ATTN AFRDQ

HEADQUARTERS
ELECTRONIC SYSTEMS DIVISION
DEPARTMENT OF THE AIR FORCE
HANSCOM AFB, MA 01731
01CY ATTN J. DEAS

HEADQUARTERS
ELECTRONIC SYSTEMS DIVISION/YSEA
DEPARTMENT OF THE AIR FORCE
HANSCOM AFB, MA 01732
01CY ATTN YSEA

HEADQUARTERS
ELECTRONIC SYSTEMS DIVISION/DC
DEPARTMENT OF THE AIR FORCE
HANSCOM AFB, MA 01731
01CY ATTN DCKC MAJ J.C. CLARK

COMMANDER
FOREIGN TECHNOLOGY DIVISION, AFSC
WRIGHT-PATTERSON AFB, OH 45433
01CY ATTN NICD LIBRARY
01CY ATTN ETDP B. BALLARD

COMMANDER
ROME AIR DEVELOPMENT CENTER, AFSC
GRIFFISS AFB, NY 13441
01CY ATTN DOC LIBRARY/TSLD
01CY ATTN OCSE V. COYNE

SAMSO/SZ
POST OFFICE BOX 92960
WORLDWAY POSTAL CENTER
LOS ANGELES, CA 90009
(SPACE DEFENSE SYSTEMS)
01CY ATTN SZJ

STRATEGIC AIR COMMAND/XPFS
OFFUTT AFB, NB 68113
01CY ATTN ADWATE MAJ BRUCE BAUER
01CY ATTN NRT
01CY ATTN DOK CHIEF SCIENTIST

SAMSO/SK
P.O. BOX 92960
WORLDWAY POSTAL CENTER
LOS ANGELES, CA 90009
01CY ATTN SKA (SPACE COMM SYSTEMS)
M. CLAVIN

SAMSO/MN
NORTON AFB, CA 92409
(MINUTEMAN)
01CY ATTN MNNL

COMMANDER
ROME AIR DEVELOPMENT CENTER, AFSC
HANSCOM AFB, MA 01731
01CY ATTN EEP A. LORENTZEN

DEPARTMENT OF ENERGY
LIBRARY ROOM G-042
WASHINGTON, D.C. 20545
01CY ATTN DOC CON FOR A. LABOWITZ

DEPARTMENT OF ENERGY
ALBUQUERQUE OPERATIONS OFFICE
P.O. BOX 5400
ALBUQUERQUE, NM 87115
01CY ATTN DOC CON FOR D. SHERWOOD

EG&G, INC.
LOS ALAMOS DIVISION
P.O. BOX 809
LOS ALAMOS, NM 85544
01CY ATTN DOC CON FOR J. BREEDLOVE

UNIVERSITY OF CALIFORNIA
LAWRENCE LIVERMORE LABORATORY
P.O. BOX 808
LIVERMORE, CA 94550
01CY ATTN DOC CON FOR TECH INFO DEPT
01CY ATTN DOC CON FOR L-389 R. OTT
01CY ATTN DOC CON FOR L-31 R. HAGER
01CY ATTN DOC CON FOR L-46 F. SEWARD

LOS ALAMOS NATIONAL LABORATORY
P.O. BOX 1663
LOS ALAMOS, NM 87545
01CY ATTN DOC CON FOR J. WOLCOTT
01CY ATTN DOC CON FOR R.F. TASCHEK
01CY ATTN DOC CON FOR E. JONES
01CY ATTN DOC CON FOR J. MALIK
01CY ATTN DOC CON FOR R. JEFFRIES
01CY ATTN DOC CON FOR J. ZINN
01CY ATTN DOC CON FOR P. KEATON
01CY ATTN DOC CON FOR D. WESTERVELT
01CY ATTN D. SAPPENFIELD

SANDIA LABORATORIES
P.O. BOX 5800
ALBUQUERQUE, NM 87115
01CY ATTN DOC CON FOR W. BROWN
01CY ATTN DOC CON FOR A. THORNBROUGH
01CY ATTN DOC CON FOR T. WRIGHT
01CY ATTN DOC CON FOR D. DAHLGREN
01CY ATTN DOC CON FOR 3141
01CY ATTN DOC CON FOR SPACE PROJECT DIV

SANDIA LABORATORIES
LIVERMORE LABORATORY
P.O. BOX 969
LIVERMORE, CA 94550
01CY ATTN DOC CON FOR B. MURPHEY
01CY ATTN DOC CON FOR T. COOK

OFFICE OF MILITARY APPLICATION
DEPARTMENT OF ENERGY
WASHINGTON, D.C. 20545
01CY ATTN DOC CON DR. YO SONG

OTHER GOVERNMENT

DEPARTMENT OF COMMERCE
NATIONAL BUREAU OF STANDARDS
WASHINGTON, D.C. 20234
01CY (ALL CORRES:
ATTN SEC OFFICER FOR)

INSTITUTE FOR TELECOM SCIENCES
NATIONAL TELECOMMUNICATIONS & INFO ADMIN
BOULDER, CO 80303
01CY ATTN A. JEAN (UNCLASS ONLY)
01CY ATTN W. UTLAUT
01CY ATTN D. CROMBIE
01CY ATTN L. BERRY

NATIONAL OCEANIC & ATMOSPHERIC ADMIN
ENVIRONMENTAL RESEARCH LABORATORIES
DEPARTMENT OF COMMERCE
BOULDER, CO 80302
01CY ATTN R. GRUBB
01CY ATTN AERONOMY LAB G. REID

DEPARTMENT OF DEFENSE CONTRACTORS

AEROSPACE CORPORATION
P.O. BOX 92957
LOS ANGELES, CA 90009
01CY ATTN I. GARFUNKEL
01CY ATTN T. SALMI
01CY ATTN V. JOSEPHSON
01CY ATTN S. BOWER
01CY ATTN D. OLSEN

ANALYTICAL SYSTEMS ENGINEERING CORP
5 OLD CONCORD ROAD
BURLINGTON, MA 01803
01CY ATTN RADIO SCIENCES

AUSTIN RESEARCH ASSOC., INC.
1901 RUTLAND DRIVE
AUSTIN, TX 78758
01CY ATTN L. SLOAN
01CY ATTN R. THOMPSON

BERKELEY RESEARCH ASSOCIATES, INC.
P.O. BOX 983
BERKELEY, CA 94701
01CY ATTN J. WORKMAN
01CY ATTN C. PRETTIE
01CY ATTN S. BRECHT

BOEING COMPANY, THE
P.O. BOX 3707
SEATTLE, WA 98124
01CY ATTN G. KEISTER
01CY ATTN D. MURRAY
01CY ATTN G. HALL
01CY ATTN J. KENNEY

CHARLES STARK DRAPER LABORATORY, INC.
555 TECHNOLOGY SQUARE
CAMBRIDGE, MA 02139
01CY ATTN D.B. COX
01CY ATTN J.P. GILMORE

COMSAT LABORATORIES
LINTHICUM ROAD
CLARKSBURG, MD 20734
01CY ATTN G. HYDE

CORNELL UNIVERSITY
DEPARTMENT OF ELECTRICAL ENGINEERING
ITHACA, NY 14850
01CY ATTN D.T. FARLEY, JR.

ELECTROSPACE SYSTEMS, INC.
BOX 1359
RICHARDSON, TX 75080
01CY ATTN H. LOGSTON
01CY ATTN SECURITY (PAUL PHILLIPS)

EOS TECHNOLOGIES, INC.
606 Wilshire Blvd.
Santa Monica, Calif 90401
01CY ATTN C.B. GABBARD

ESL, INC.
495 JAVA DRIVE
SUNNYVALE, CA 94086
01CY ATTN J. ROBERTS
01CY ATTN JAMES MARSHALL

GENERAL ELECTRIC COMPANY
SPACE DIVISION
VALLEY FORGE SPACE CENTER
GODDARD BLVD KING OF PRUSSIA
P.O. BOX 8555
PHILADELPHIA, PA 19101
01CY ATTN M.H. BORTNER SPACE SCI LAB

GENERAL ELECTRIC COMPANY
P.O. BOX 1122
SYRACUSE, NY 13201
01CY ATTN F. REIBERT

GENERAL ELECTRIC TECH
SERVICES CO., INC.
HMES
COURT STREET
SYRACUSE, NY 13201
01CY ATTN G. MILLMAN

GEOPHYSICAL INSTITUTE
UNIVERSITY OF ALASKA
FAIRBANKS, AK 99701
(ALL CLASS ATTN: SECURITY OFFICER)
01CY ATTN T.N. DAVIS (UNCLASS ONLY)
01CY ATTN TECHNICAL LIBRARY
01CY ATTN NEAL BROWN (UNCLASS ONLY)

GTE SYLVANIA, INC.
ELECTRONICS SYSTEMS GRP-EASTERN DIV
77 A STREET
NEEDHAM, MA 02194
01CY ATTN DICK STEINHOF

HSS, INC.
2 ALFRED CIRCLE
BEDFORD, MA 01730
01CY ATTN DONALD HANSEN

ILLINOIS, UNIVERSITY OF
107 COBLE HALL
150 DAVENPORT HOUSE
CHAMPAIGN, IL 61820
(ALL CORRES ATTN DAN MCCLELLAND)
01CY ATTN K. YEH

INSTITUTE FOR DEFENSE ANALYSES
1801 NO. BEAUREGARD STREET
ALEXANDRIA, VA 22311
01CY ATTN J.M. AEIN
01CY ATTN ERNEST BAUER
01CY ATTN HANS WOLFARD
01CY ATTN JOEL BENGSTON

INTL TEL & TELEGRAPH CORPORATION
500 WASHINGTON AVENUE
NUTLEY, NJ 07110
01CY ATTN TECHNICAL LIBRARY

JAYCOR
11011 TORREYANA ROAD
P.O. BOX 85154
SAN DIEGO, CA 92138
01CY ATTN J.L. SPERLING

JOHNS HOPKINS UNIVERSITY
APPLIED PHYSICS LABORATORY
JOHNS HOPKINS ROAD
LAUREL, MD 20810
01CY ATTN DOCUMENT LIBRARIAN
01CY ATTN THOMAS POTEMRA
01CY ATTN JOHN DASSOULAS

KAMAN SCIENCES CORP
P.O. BOX 7463
COLORADO SPRINGS, CO 80933
01CY ATTN T. MEAGHER

KAMAN TEMPO-CENTER FOR ADVANCED STUDIES
816 STATE STREET (P.O DRAWER QQ)
SANTA BARBARA, CA 93102
01CY ATTN DASIAC
01CY ATTN WARREN S. KNAPP
01CY ATTN WILLIAM MCNAMARA
01CY ATTN B. GAMBILL

LINKABIT CORP
10453 ROSELLE
SAN DIEGO, CA 92121
01CY ATTN IRWIN JACOBS

LOCKHEED MISSILES & SPACE CO., INC
P.O. BOX 504
SUNNYVALE, CA 94088
01CY ATTN DEPT 60-12
01CY ATTN D.R. CHURCHILL

LOCKHEED MISSILES & SPACE CO., INC.
3251 HANOVER STREET
PALO ALTO, CA 94304
01CY ATTN MARTIN WALT DEPT 52-12
01CY ATTN W.L. IMHOF DEPT 52-12
01CY ATTN RICHARD G. JOHNSON
DEPT 52-12
01CY ATTN J.B. CLADIS DEPT 52-12

MARTIN MARIETTA CORP
ORLANDO DIVISION
P.O. BOX 5837
ORLANDO, FL 32805
01CY ATTN R. HEFFNER

M.I.T. LINCOLN LABORATORY
P.O. BOX 73
LEXINGTON, MA 02173
01CY ATTN DAVID M. TOWLE
01CY ATTN L. LOUGHLIN
01CY ATTN D. CLARK

MCDONNEL DOUGLAS CORPORATION
5301 BOLSA AVENUE
HUNTINGTON BEACH, CA 92647
01CY ATTN N. HARRIS
01CY ATTN J. MOULE
01CY ATTN GEORGE MROZ
01CY ATTN W. OLSON
01CY ATTN R.W. HALPRIN
01CY ATTN TECHNICAL LIBRARY SERVICES

MISSION RESEARCH CORPORATION
735 STATE STREET
SANTA BARBARA, CA 93101
01CY ATTN P. FISCHER
01CY ATTN W.F. CREVIER
01CY ATTN STEVEN L. GUTSCHE
01CY ATTN R. BOGUSCH
01CY ATTN R. HENDRICK
01CY ATTN RALPH KILB
01CY ATTN DAVE SOWLE
01CY ATTN F. FAJEN
01CY ATTN M. SCHEIBE
01CY ATTN CONRAD L. LONGMIRE
01CY ATTN B. WHITE

MISSION RESEARCH CORP.
1400 SAN MATEO BLVD. SE
SUITE A
ALBUQUERQUE, NEW MEXICO 87108
01CY R. STELLINGWERF
01CY M. ALME
01CY L. WRIGHT

MITRE CORPORATION, THE
P.O. BOX 208
BEDFORD, MA 01730
01CY ATTN JOHN MORGANSTERN
01CY ATTN G. HARDING
01CY ATTN C.E. CALLAHAN

MITRE CORP
WESTGATE RESEARCH PARK
1820 DOLLY MADISON BLVD
MCLEAN, VA 22101
01CY ATTN W. HALL
01CY ATTN W. FOSTER

PACIFIC-SIERRA RESEARCH CORP
12340 SANTA MONICA BLVD.
LOS ANGELES, CA 90025
01CY ATTN E.C. FIELD, JR.

PENNSYLVANIA STATE UNIVERSITY
IONOSPHERE RESEARCH LAB
318 ELECTRICAL ENGINEERING EAST
UNIVERSITY PARK, PA 16802
(NO CLASS TO THIS ADDRESS)
01CY ATTN IONOSPHERIC RESEARCH LAB

PHOTOMETRICS, INC.
4 ARROW DRIVE
WOBURN, MA 01801
01CY ATTN IRVING L. KOFSKY

PHYSICAL DYNAMICS, INC.
P.O. BOX 3027
BELLEVUE, WA 98009
01CY ATTN E.J. FREMOUW

PHYSICAL DYNAMICS, INC.
P.O. BOX 10367
OAKLAND, CA 94610
ATTN A. THOMSON

R & D ASSOCIATES
P.O. BOX 9695
MARINA DEL REY, CA 90291
01CY ATTN FORREST GILMORE
01CY ATTN WILLIAM B. WRIGHT, JR.
01CY ATTN ROBERT F. LELEVIER
01CY ATTN WILLIAM J. KARZAS
01CY ATTN H. ORY
01CY ATTN C. MACDONALD
01CY ATTN R. TURCO
01CY ATTN L. DeRADD

RAND CORPORATION, THE
1700 MAIN STREET
SANTA MONICA, CA 90406
01CY ATTN CULLEN CRAIN
01CY ATTN ED BEDROZIAN

RAYTHEON CO.
528 BOSTON POST ROAD
SUDBURY, MA 01776
01CY ATTN BARBARA ADAMS

RIVERSIDE RESEARCH INSTITUTE
80 WEST END AVENUE
NEW YORK, NY 10023
01CY ATTN VINCE TRAPANI

SCIENCE APPLICATIONS, INC.
P.O. BOX 2351
LA JOLLA, CA 92038
01CY ATTN LEWIS M. LINSON
01CY ATTN DANIEL A. HAMLIN
01CY ATTN E. FRIEMAN
01CY ATTN E.A. STRAKER
01CY ATTN CURTIS A. SMITH
01CY ATTN JACK MCDOUGALL

SCIENCE APPLICATIONS, INC
1710 GOODRIDGE DR.
MCLEAN, VA 22102
ATTN: J. COCKAYNE

SRI INTERNATIONAL
333 RAVENSWOOD AVENUE
MENLO PARK, CA 94025
01CY ATTN DONALD NEILSON
01CY ATTN ALAN BURNS
01CY ATTN G. SMITH
01CY ATTN R. TSUNODA
01CY ATTN DAVID A. JOHNSON
01CY ATTN WALTER G. CHESNUT
01CY ATTN CHARLES L. RINO
01CY ATTN WALTER JAYE
01CY ATTN J. VICKREY
01CY ATTN RAY L. LEADABRAND
01CY ATTN G. CARPENTER
01CY ATTN G. PRICE
01CY ATTN R. LIVINGSTON
01CY ATTN V. GONZALES
01CY ATTN D. MCDANIEL

TECHNOLOGY INTERNATIONAL CORP
75 WIGGINS AVENUE
BEDFORD, MA 01730
01CY ATTN W.P. BOQUIST

TOYON RESEARCH CO.
P.O. Box 6890
SANTA BARBARA, CA 93111
01CY ATTN JOHN ISE, JR.
01CY ATTN JOEL GARBARINO

TRW DEFENSE & SPACE SYS GROUP
ONE SPACE PARK
REDONDO BEACH, CA 90278
01CY ATTN R. K. PLEBUCH
01CY ATTN S. ALTSCHULER
01CY ATTN D. DEE
01CY ATTN D/ STOCKWELL
SNTF/1575

VISIDYNE
SOUTH BEDFORD STREET
BURLINGTON, MASS 01803
01CY ATTN W. REIDY
01CY ATTN J. CARPENTER
01CY ATTN C. HUMPHREY

DOE DISTRIBUTION LIST FOR REPORTS

University of California
Lawrence Livermore National Lab
Post Office Box 808
Livermore, CA 94550
H.G. Ahlstrom, L-481
J.L Emmett, L-448
J.F. Holzrichter, L-481
M.J. Monsler, L-479
J.H. Nuckolls, L-477
L.W. Coleman, L-473
J.T. Hunt, L-481
A.B. Langdon, L-477

U.S. Department of Energy
Office of Inertial Fusion
Washington, DC 20545
L.E. Killian
G. Gibbs
T.F. Godlove
S.L. Kahalas
J.E. Lewis
R.L. Schriever
T.H. Walsh
S.J. Barish

U.S. Dept. of Energy (194 cys)
Technical Information Center
P.O. Box 62
Oak Ridge, TN 37830

Defense Tech. Information Ctr. (2 cys)
Cameron Station
5010 Duke Street
Alexandria, VA 22314

R. McCrory
University of Rochester
250 East River Road
Rochester, NY 14623

Robert T. Duff
U.S. Department of Energy
Office of Classification
Washington, DC 20545

Rex B. Purcell (2 cys)
U.S. Department of Energy
Nevada Operations Office
Post Office Box 14100
Las Vegas, NV 89114

Z.N. Zafiris/R. Bredderman
U.S. Department of Energy
San Francsico Operations Office
1333 Broadway
Oakland, CA 94512

Los Alamos National Laboratory
Post Office Box 1663
Los Alamos, NM 87545
S.D. Rockwood, ICF Prog. Mgr.
DAD/IF, M/S527 (6 cys)

G. Yonas (4 cys)
Sandia National Laboratories
Post Office Box 5880
Albuquerque, NM 87185

S. Bodner
Naval Research Laboratory
Code 4730
Washington, DC 20375

T. Coffey
Naval Research Laboratory
Code 1001
Washington, DC 20375

Alexander Glass
KMS Fusion, Inc.
3941 Research Park Drive
P.O. Box 1567
Ann Arbor, MI 48106

NRL Code 4700 (26 cys)

NRL Code 4730 (200 cys)

NRL Code 2628 (22 cys)

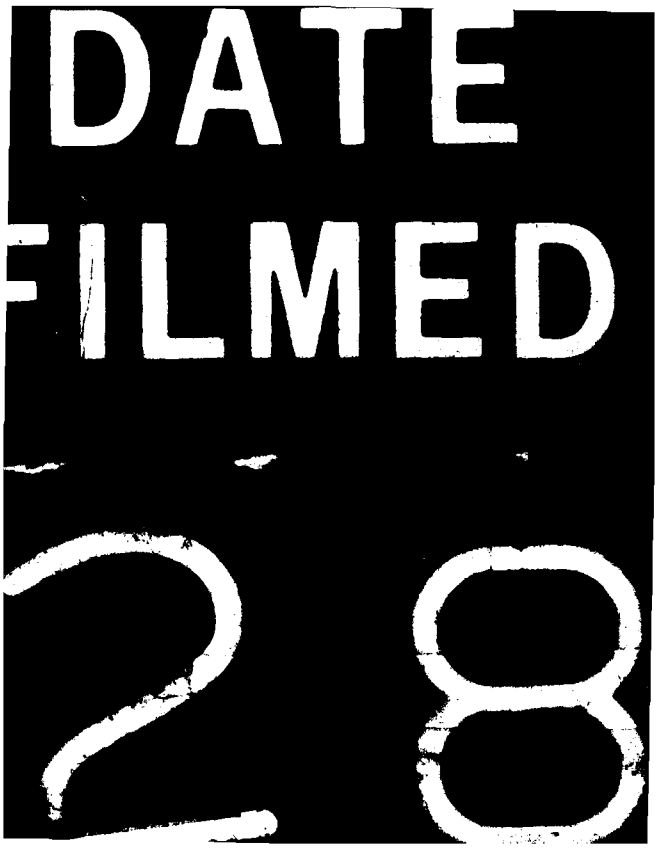
DATE
FILMED
28